RSC Advances

PAPER

View Article Online
View Journal | View Issue

Cite this: *RSC Adv.*, 2024, **14**, 2429

Enhancement of the photocatalytic activity of rGO/NiO/Ag nanocomposite for degradation of methylene blue dye

Durgesh Singh,[a] Khalid Mujasam Batoo,[b] Sajjad Hussain,[cd] Anjan Kumar,[e] Qusay Husam Aziz,*[f] Fatime Satar Sheri,[g] Hayder Tariq[h] and Parminder Singh[i]

Received 14th October 2023
Accepted 4th January 2024

DOI: 10.1039/d3ra07000j

rsc.li/rsc-advances

The current study focuses on boosting the photocatalytic ability of reduced graphene oxide (rGO) by decorating the rGO nano-sheets with nickel oxide (NiO_x) and silver (Ag) nanomaterials. The developed ternary nanomaterials were investigated using FTIR, XRD, FESEM, TEM, Raman, and UV-vis to evaluate the photo-degradation process. The rGO/NiO_x/Ag ternary system showed promising photocatalytic dye degradation under simulated sunlight irradiance. The addition of NiO_x and Ag nanomaterials widened the catalytic activity spectrum from the visible region to the UV-region. Besides, these materials hindered the electron–hole recombination, boosting the catalytic activity. The reusability results also clearly showed that the synthesized ternary nanomaterials have good reproducibility and stability for photocatalytic degradation of industrial wastewater.

Introduction

For our life on earth, we all rely on clean water. Regardless, the increasing industrial and residential contaminants that are regularly discharged into natural water supplies pollute the ecosystem. Several research studies have reported that 12% of dyes used in textile industries, including Rose Bengal, Rhodamine B, Methylene Blue (MB), Indigo Red, Caramine, Victoria blue, Red 120, Thymol blue, Eriochrome, Methylene Blue (MB), and Black-T (EBT),[1–5] are lost throughout the production and processing actions and end up in wastewater.[6] Such dye-polluted wastewater contains non-biodegradable, extremely toxic, and colored pigments which can be toxic and detrimental to living creatures.[7,8] This has prompted scholars from all around the world to work together to tackle the problem by developing effective methods to clean or treat the water. Polluted water may be efficiently cleansed by decomposing organic contaminants in a safe and environmentally benign manner utilizing a photocatalytic degradation method.[9–13]

Due to their low cost, good stability, environmental friendliness, and non-toxicity, semiconductor photocatalysts have sparked a lot of interest in the degradation of organic pollutants over the last decade.[14] Semiconductor metal oxide nanoparticles have been proposed to be efficient photocatalysts for photo-degradation.[15,16] Among the numerous semiconductor metal oxide nanoparticles, nickel oxide (NiO_x) nanoparticles with a band gap of 3.6–4.0 eV were chosen as a photocatalyst.[17,18] It is an important material in environmental research because of its multiple applications in the breakdown of inorganic contaminants, poisonous dyes, and the biological sector. However, its low light transmittance, coagulation proclivity, and poor dispersibility restrict its efficiency[19] limiting its use in a variety of environmental issues. This disadvantage creates opportunities for progress in this field. Because of their outstanding photocatalytic activity, metal oxide, graphene/noble metal/metal oxide, and metal oxide nanohybrids have received a lot of interest. Carbon nanostructures like graphene, fullerenes, carbon nanotubes, and carbon ribbon-based nanocomposites are gaining popularity in photovoltaics, photocatalysis, and energy storage devices.[20]

The reduced graphene oxide (rGO) is used to serve as a catalyst for a variety of reasons, including its high surface area, strong light absorption, and good electron mobility.[21–24] Various studies on connecting rGO to suitable semiconductors have additionally been conducted. The charge transport properties of carbon, as well as its electronic interaction with a semiconductor, enable some novel electrical and photocatalytic uses. The incorporation of well-known metals/metal sulfides/

[a]*Department of Chemistry, School of Chemical Sciences and Technology, Dr.Harisingh Gour Vishwavidyalaya (A Central University), Sagar, 470003, Madhya Pradesh, India*
[b]*College of Science, King Saud University, P.O. Box-2455, Riyadh 11451, Saudi Arabia*
[c]*Hybrid Materials Center (HMC), Sejong University, Seoul 05006, Republic of Korea*
[d]*Department of Nanotechnology and Advanced Materials Engineering, Sejong University, Seoul 05006, Republic of Korea*
[e]*Department of ECE, GLA University, Mathura 281406, India*
[f]*Department of Anesthesia Techniques, Al-Noor University College, Nineveh, Iraq. E-mail: qusay.husam@alnoor.edu.iq*
[g]*National University of Science and Technology, Dhi Qar, Iraq*
[h]*Department of Pharmacy, Al-Zahrawi University College, Karbala, Iraq*
[i]*Chemical Engineering Department, Thapar Institute of Engineering and Technology, Patiala, India*

metal oxides catalytic nanomaterials with materials made from graphene results in higher efficiency over the materials in their naked state. In graphene/metal oxide photocatalytic composites, graphene is used as a charge acceptor and transporter, an enhanced photons absorber, and an extensive surface host and support.[11,25–27] Because of graphene's electrical conductivity, charge carriers obtained during photoexcitation can be accepted quickly, resulting in less electron–hole pair recombination. The processes such as doping, composite creation, dye sensitization, and noble metal inclusion are favored techniques for activating photocatalytic materials in the visible region.[28–33] Surface plasmon resonance (SPR) behaviour has been found to cause the aforementioned properties in Ag or Au anchored ZnO-based heterostructures.[30,33]

After taking into account all of these parameters, we propose combining all three components (NiO_x, rGO, and Ag) to improve photocatalytic activity by lengthening electron–hole pair separation rate and improving visible light area functioning.[32,34,35] As a result, a hydrothermal method was used to create a rGO/NiO_x hybrid composite. The Ag nanoparticles were coated on rGO/NiO_x as rGO/NiO_x/Ag and the resulting materials were tested for photocatalytic activity. Through ultraviolet-visible diffuse reflectance (UV-vis) spectroscopy, the basic roles of as-synthesized rGO, rGO/NiO_x, and rGO/NiO_x/Ag nanocomposites in the photocatalytic process were examined in detail. Under UV light irradiation, the rGO/NiO_x/Ag nanocomposite improved photocatalytic activity towards the destruction of methylene blue dye. As a result, the degradation efficiency of methylene blue dye in rGO/NiO_x/Ag nanocomposite was 91%, much above that of rGO/NiO_x. The higher photocatalytic activity of the rGO/NiO_x/Ag composites was mostly owing to improved carrier separation efficiency, according to our findings.

Materials and method

Synthesis of rGO nano-sheets

500 mg of graphite powder (99%, Alfa Aesar) were placed in a beaker followed by addition of 25 mL sulfuric acid (98%, Merck) while stirring at temperature of 2 °C. Then, 1.5 g potassium permanganate (99%, Merck) was poured to the solution at temperature of 10 °C. Then, the graphite solution was stirred at RT for 45 min. After that, 200 mL distilled water (DW) was added into the beaker, followed by extra 2 h ultrasonic treatment. By adding sodium hydroxide (98%, Merck) solution (1 M), the pH of suspension was adjusted at 6, followed by sonication for 1 h. 5 g L-ascorbic acid (99%, Merck) was poured in 50 mL DW and was drop wised to the graphite oxide solution at RT. These solution was stirred at 95 °C for 120 min for reduction of graphite oxide. The obtained precipitates were filtered and washed with DW and a 1 M HCl solution (37%, Merck) to reduce pH to neutral. Finally, the washed precipitates were dried at temperature of 40 °C for 48 h to obtain rGO nano-sheets.

Synthesis of rGO/NiO_x hybrid composite

713 mg of nickel nitrate hexahydrate ($Ni(NO_3)_2 \cdot 6H_2O$, 99%, Merck) and 360 mg urea (99%, Merck) were dissolved to 6 mL of DW (solution A) with assistance of sonication at RT for 30 min. 300 mg rGO powder was added in 150 mL DW in a beaker and sonicated for 1 h at temperature of 40 °C (solution B). Then, solution B put on a magnetic stirrer and whole of solution A was drop wised to it. The final solution was kept on constant stirring for 2 h at RT. The obtained solution was transferred into a Teflon autoclave, and maintained at 150 °C for 8 h. After that, the resultant was washed with ethanol and DW and dried in an oven at 60 °C overnight. Finally, the obtained powders were annealed at 300 °C for 3 h to product rGO/NiO_x composite.

Synthesis of Ag nanoparticles

Silver nanoparticles were synthesized as follow. Typically, 444 mg of polyvinylpyrrolidone (PVP, MW40000, Merck) was poured to 40 mL of polyethylene glycol (PEG, MW600, Merck) and stirred at 80 °C for 4 h. After that, 1 mL of $AgNO_3$ solution in DW (0.5 M) was promptly injected to the above solution, followed by continue stirring at 80 °C to change the color of the solution from colorless to light yellow. The obtained solution was transferred to Teflon autoclave and kept at temperature of 220 °C for 24 h. After cooling down the solution to RT, it was centrifuged for 10 min to separate product from the surfactants and PEG. To further purification, the obtained Ag NPs were dissolved in DW and ethanol and centrifuged several times. Finally, the product was dried at 50 °C overnight.

Synthesis of rGO/NiO_x/Ag ternary nanocomposites

The rGO/NiO_x/Ag nanocomposite was synthesized *via* a hydrothermal method. 100 mg rGO/NiO_x hybrid composite was dispersed in 50 mL deionized water by sonication at RT for 45 min. 10 mg Ag NPs was dispersed in 50 mL deionized water by sonication at RT for 30 min. The Ag dispersion was added to the rGO/NiO_x solution. The slurry suspension liquid was refluxed at 90 °C for 24 h. Next, the prepared colloid was centrifuged and washed by deionized water several times and finally dried at 60 °C overnight. Fig. 1 shows schematic diagram of rGO/NiO_x and rGO/NiO_x/Ag materials.

Photocatalytic activity of MB

Photocatalytic ability of materials for MB degradation was measured *via* recording of absorbance spectra trends *versus* time, while they were irradiated with a simulated sunlight. 50 mg of various nanomaterials (rGO, rGO/NiO_x, and rGO/NiO_x/Ag) were poured into 100 mL MB dye solution (10 ppm). Then, solutions were kept at dark conditions for 45 min, followed by exposing to illumination and recording UV-vis responses. The photocatalyst stability of rGO/NiO_x/Ag material was investigated by running the photocatalytic reaction for 4 different times employing the same catalyst. 50 mg of the rGO/NiO_x/Ag catalyst mixed in 100 mL of MB dye solution was centrifuged at 3000 rpm for 5 min after the final reaction. The recovered catalyst was again used for the second time after washing and

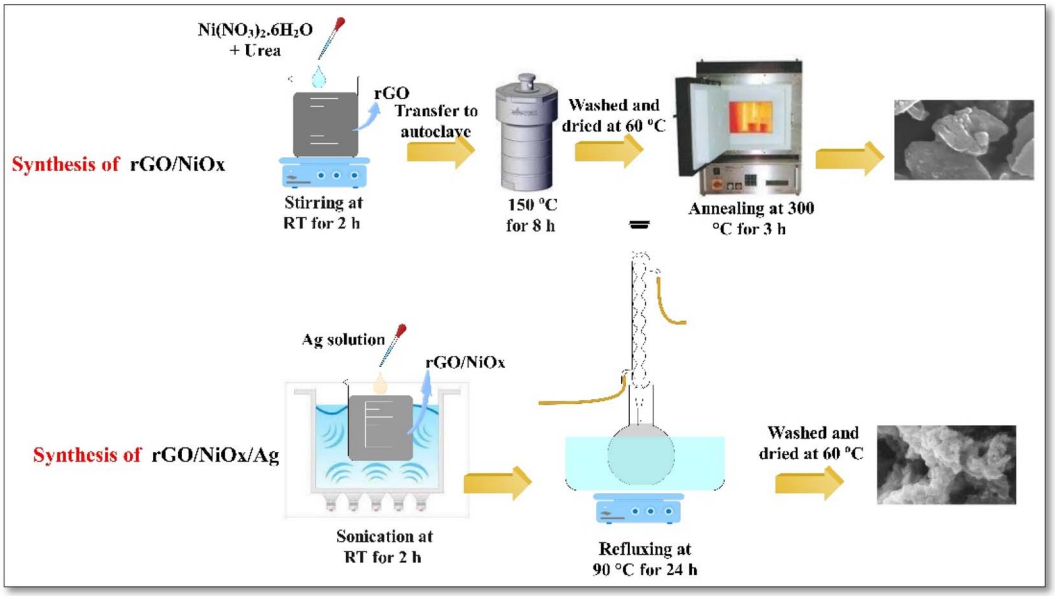

Fig. 1 Schematic diagram for synthesis of rGO/NiO_x and rGO/NiO_x/Ag materials.

heating at 75 °C, 6 h. This process was repeated for two more times to complete the reusability MB degradation performance of the rGO/NiO_x/Ag system.

Characterization

TEM and FE-SEM images of materials were recorded with Philips BioTwin CM120 and TESCAN MIRA 3 instruments, respectively. Bruker, D8 advance X-ray diffractometer was employed to collect X-ray diffraction (XRD) patterens of materials. Absorbance spectra of samples were investigated with an LINE9600 spectrometer in a wavelength range of 200–800 nm. RAMAN spectra of materials were recorded with a Raman Ram-532-004 device. PL spectra of samples were collected with a PL CARY ECLIPSE spectrophotometer. Bet responses of samples were measured using a BELSORP Mini II device.

Results

Fig. 2a depicts the UV-vis absorption spectra of rGO, Ag-NPs, NiO_x-NPs, rGO/NiO_x, and rGO/NiO_x/Ag nanocomposite. Pure NiO_x nanoparticles show absorption in the UV region at 317 nm, where electrons move from the oxygen band to the NiO_x valence band.[36] Therefore, rGO/NiO_x shows a higher absorption intensity than NiO_x nanoparticles and pure rGO. When rGO/NiO_x/Ag nanocomposite was compared to rGO/NiO_x, the absorption edge was red-shifted. The absorption peaks appearing at 264 and 312 nm (Fig. 2a) confirm the formation of rGO/NiO_x/Ag nanocomposite. In addition, by incorporation of Ag NPs on the rGO/NiO_x surface, a shoulder peak at 400 nm is observed, which correlates to the local surface plasmon resonance (LSPR) of Ag NPs. The presence of Ag NPs on the rGO/NiO_x material thanks to their LSPR increases the visible light absorption and assists to increase photocatalytic activity.[37,38] The Tauc plot was used to measure synthesized samples' bandgap (E_g).[39] Pure rGO has a bandgap of 1.59 eV, which is changed to 2.71 eV after NiO_x is added to the rGO lattice (Fig. 2b). After inserting Ag into the rGO/NiO_x lattice, the bandgap value of rGO/NiO_x dropped to 2.51 eV. The narrow band gap of the rGO/NiO_x/Ag nanocomposite connects rGO/NiO_x and Ag, which causes Fermi levels between the valence and conduction bands.[40] Doping Ag decreases the rGO/NiO_x-based photocatalyst's optical bandgap and increases its absorption limit toward visible light.[41] These photocatalysts benefit greatly from visible light and can outperform UV-only catalysts in terms of degrading activity.[42–44]

The crystal structure of the nanocomposite was characterized by X-ray diffraction study. Fig. 2c depicts the XRD patterns of synthesized Ag-NPs, rGO, NiO_x-NPs, rGO/NiO_x, and rGO/NiO_x/Ag nanocomposites. It was found that the pure NiO_x had sharp peaks at 37.20°, 43.42°, and 63.09°. The positions of all the peaks can be indexed to the cubic phase of NiO_x (CPDS card no. 73-1519) and correspond too (111), (200), and (220).[36] In the case of the rGO/NiO_x nanocomposite, a new peak at 26.4° appeared, which corresponds to the decreased GO's (002) crystal plane.[45] It is also found that, as the Ag-NPs incorporate, a notable peak shift is evident in the XRD pattern (Fig. 2d), confirming the incorporation of Ag into the crystal lattice of rGO/NiO_x.

Fig. 3 depicts the Raman spectra of rGO, rGO/NiO_x, and rGO/NiO_x/Ag nanocomposites. Peaks for D and G bands were observed in rGO, rGO/NiO_x, and rGO/NiO_x/Ag nanocomposites, confirming the presence of sp^3 hybridised carbon atoms with disordered bonding with oxygen atoms as D band at 1364 cm^{-1} and ordered sp^2 hybridised carbon atoms as G band at 1596 cm^{-1} relating to A_{1g} symmetry.[46,47] Because of the one phonon (1P) mode of 1LO, the NiO_x in the rGO/NiO_x and rGO/NiO_x/Ag nanocomposites displayed a high-intensity Raman peak at 487 cm^{-1}.[48] The computed D band and G band intensity ratios for rGO, rGO/NiO_x, and rGO/NiO_x/Ag nanocomposites

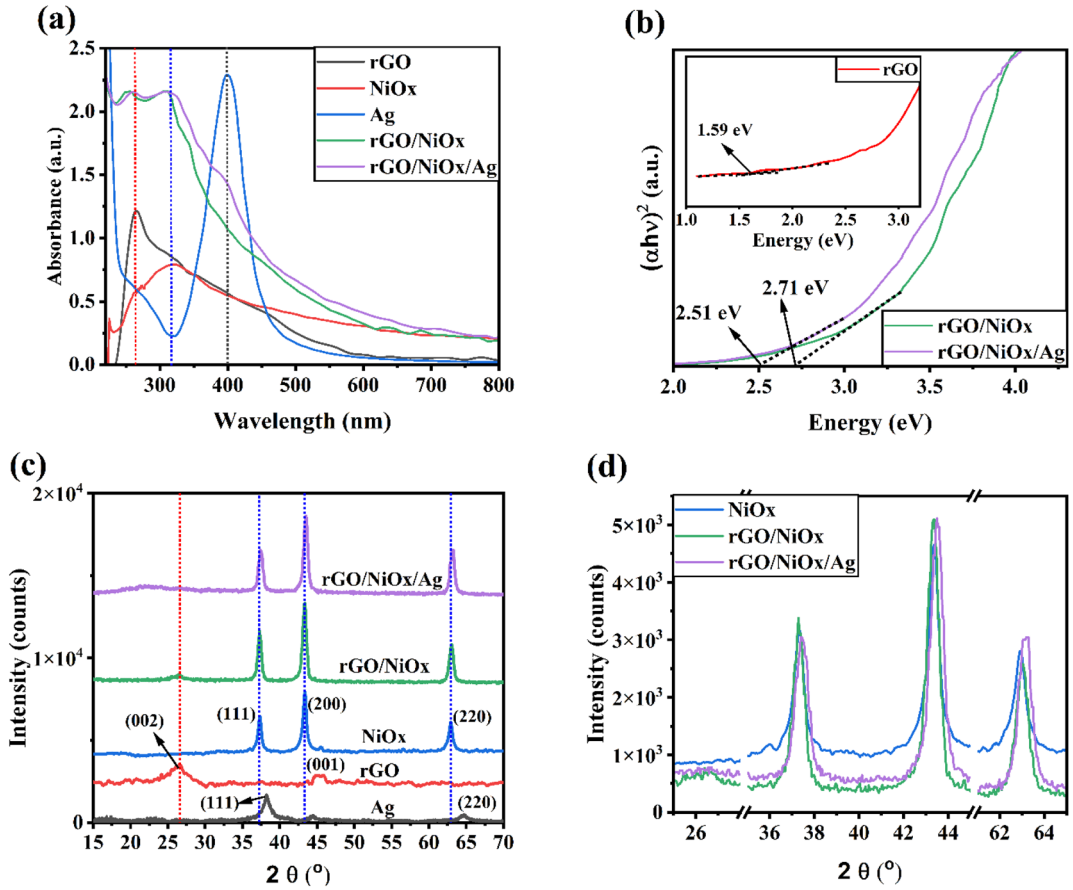

Fig. 2 (a) Absorbance spectra, (b) Tauc, (c) XRD patterns, (d) zoomed view XRD patterns of different materials.

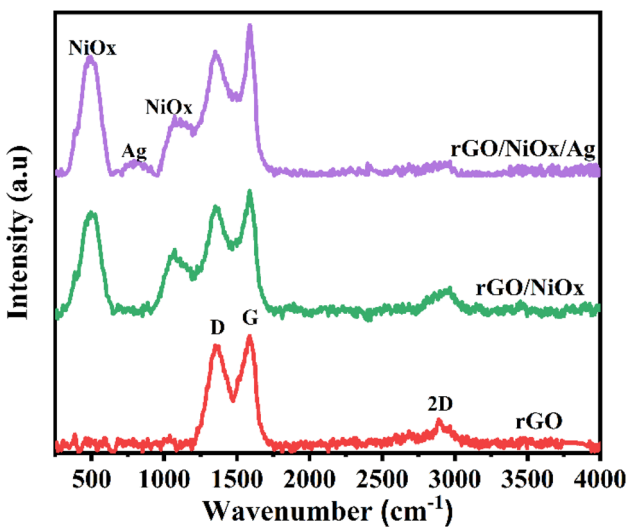

Fig. 3 RAMAN spectra of different materials.

were 0.910, 0.869, and 0.823, respectively. The intensity ratio difference can be attributed to the interaction of rGO with NiO_x–Ag, implying the formation of the nanocomposite. In addition, the reduced I_D/I_G ratio in the rGO/NiO_x/Ag can be correlated to improved conductivity, which has benefits for photocatalytic activity.

The structure and morphology of the Ag-NPs, rGO, NiO_x, rGO/NiO_x, and rGO/NiO_x/Ag nanocomposite were determined by FE-SEM (Fig. 4). As shown in Fig. 4a, the morphology of the Ag-NPs nanoparticles is approximately spherical. rGO imaging with FESEM indicated a flat, 2D substance with a severely wrinkled surface (Fig. 4b). The rGO wrinkles are created by the reduction step, which sticks the graphene sheets together and results in a crumpled shape. This crumpled shape can increase surface area and enable molecule and ion adsorption, making rGO a viable material for application in photocatalytic of industrial wastewaters.[49] The surface of NiO_x-NPs shows spherical-shaped grains with uniform diameters packed together (Fig. 4c). The NiO_x-NPs covered on the reduced graphene oxide are shown in Fig. 4d. The image clearly demonstrates the formation of tiny nanoparticles on the surface of the reduced GO sheets. The NiO_x-NPs are practically all the same size, and their dispersion is uniform across the surface of the nanosheets. Improved morphology with a uniform, formed structure with multiple holes is visible for the rGO/NiO_x/Ag ternary composites (Fig. 4e).

Fig. 5 shows elemental mapping images for the elements C, O, Ni, and Ag. The mapping study clearly demonstrates that the

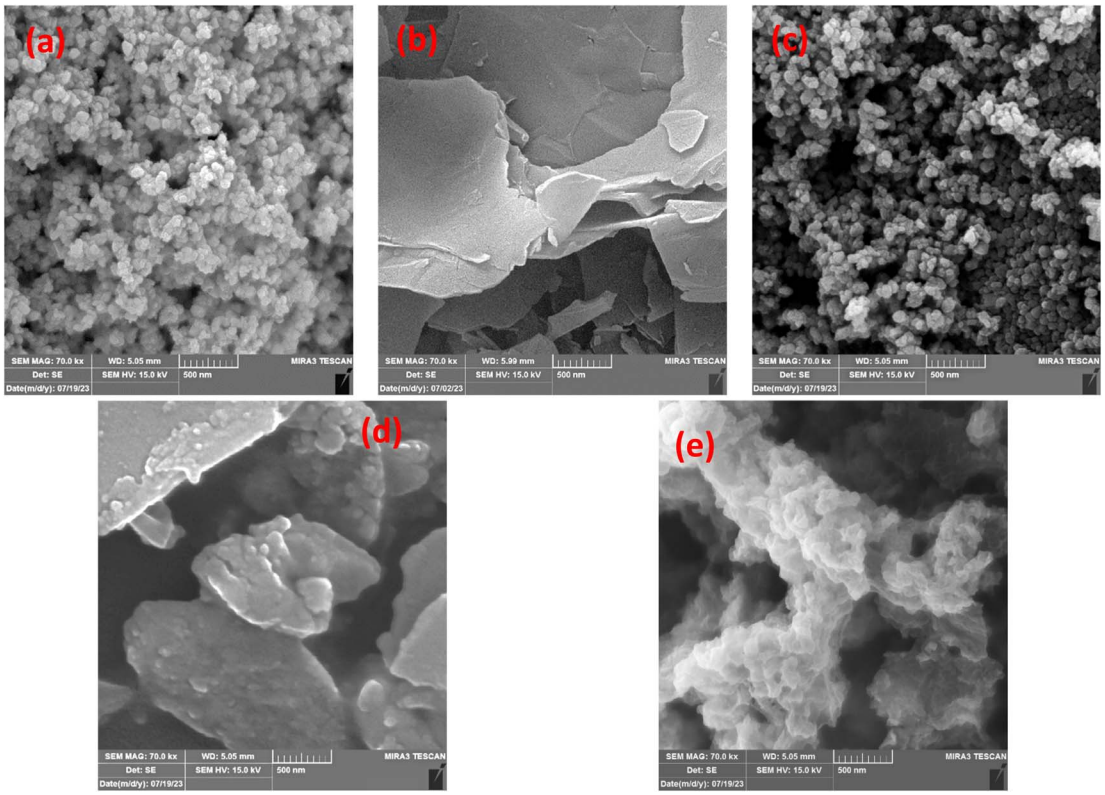

Fig. 4 FE-SEM image of (a) Ag nanoparticles, (b) rGO sheets, (c) NiO_x nanoparticles, (d) rGO/NiO_x composites, and (e) rGO/NiO_x/Ag ternary composites.

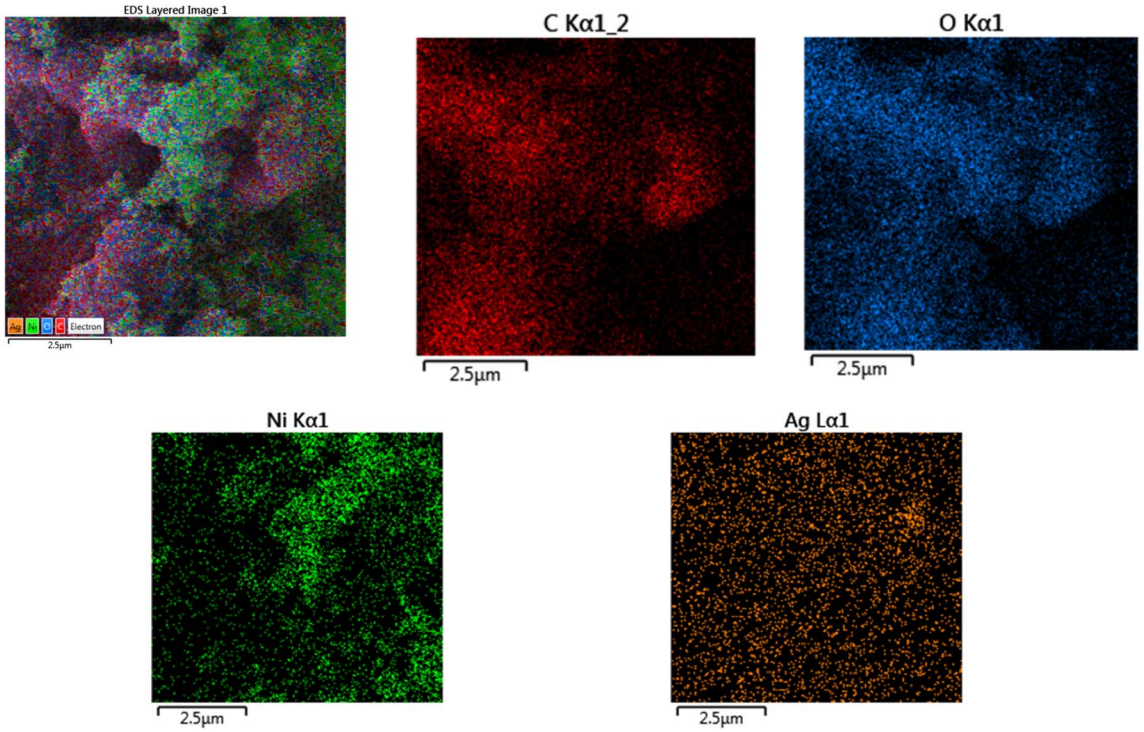

Fig. 5 Mapping FESEM to show elements distribution in rGO/NiO_x/Ag ternary composite.

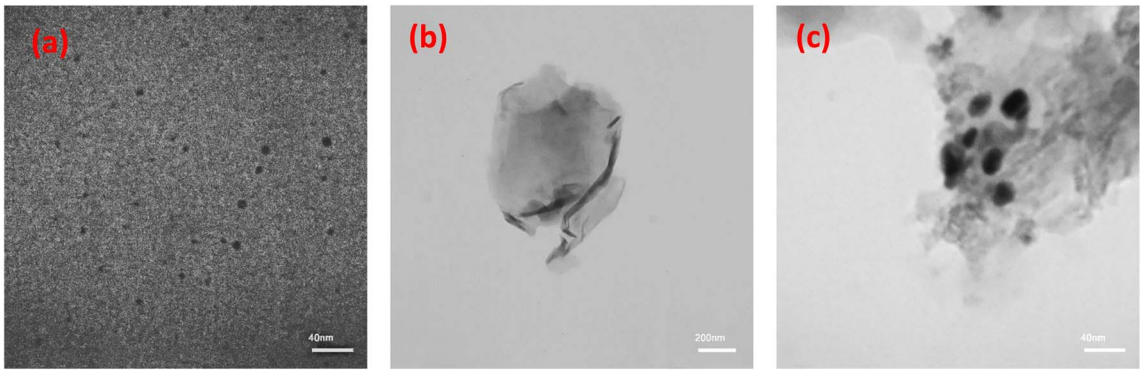

Fig. 6 TEM images of (a) Ag nanoparticles, (b) rGO sheets and (c) rGO/NiO/Ag ternary composites.

NiO_x–Ag-NPs are evenly dispersed across the entire surface of these rGO sheets.

Using TEM images, we can gain knowledge about the morphology and form of this nanocomposite (Fig. 6). Fig. 6 shows TEM image of Ag NPs, where they have sizes smaller than 10 nm. The size of Ag NPs from TEM image agrees with the obtained size for them from XRD pattern using Scherrer equation (size of ~7 nm). Fig. 6b represents the exfoliated rGO sheet, whereas NiO_x and Ag nanoparticles, anchored on the rGO nanosheet (Fig. 6c). Small spherical structures of NiO_x and Ag attached to rGO sheets appear to be appropriate for avoiding GO photoreduction. The FE-SEM images were validated by the TEM images.

We focus on the photo-assisted catalytic degradation of commercial methylene blue dye by rGO, rGO/NiO_x, and rGO/NiO_x/Ag nanocomposite. We expect that this material will show some advantages in phtocatalytic activity to limit the electron–hole recombination rate as well as enhance redox reactions because of its enhanced conductivity, chemical resistance resulting from NiO_x and Ag connection with rGO, and suitable band gap for collecting visible photons. Photocatalytic activities of pure rGO, rGO/NiO_x, and rGO/NiO_x/Ag nanocomposites were assessed through methylene blue dye degradation. Fig. 7a depicts the degradation efficiency of methylene blue dye in different reaction systems. The photodegradation efficiency of methylene blue dye, on the other hand, was just 56% for pure rGO. The quick electron–hole pair recombination may explain rGO's low photocatalytic activity. As expected, rGO/NiO_x demonstrated higher photoactivity than pure rGO, demonstrating that the addition of NiO_x to rGO promoted charge carrier separation and increased rGO's photocatalytic properties.

Interestingly, the rGO/NiO_x/Ag nanocomposite had the highest degradation efficacy (91%) in degrading methylene blue dye, possibly due to the smallest recombination of photoinduced carriers of charge (Fig. 7a). The findings showed that the nanocomposite synthesized by silver decorating to rGO/NiO_x nanocomposite was able to absorb visible light to produce carriers and degrade the methylene blue dye. The measurement of the rate constant findings (Fig. 7b) reveals that the rGO/NiO_x/Ag nanocomposite has a high rate constant, which is due to its narrow optical bandgap, robust light absorption, and minimal electron–hole recombination.

The possible photocatalytic mechanism of the rGO/NiO_x/Ag sample is depicted in Fig. 7c. By exposing simulated sunlight to the rGO/NiO_x/Ag system, the LSPR is induced in Ag NPs, which contributes to form hot electrons in the ternary system. These electrons can be inject into the conduction band of NiO_x and then transferred to the rGO surface. Injected electrons react with O_2 and generate superoxide radicals ($O_2^{\cdot}$), which later contribute to the generation of hydroxyl radicals ($^{\cdot}OH$). On the other hand, the holes from the rGO sheets can transfer to the valence band of NiO_x material, which contributes to the oxidization of H_2O/OH^- to form $^{\cdot}OH$ radicals. In continue, these $O_2^{\cdot}$ and $^{\cdot}OH$ radicals react with MB dye molecules (RH) to degrade them into non-hazardous compounds.[50,51] The reactions involved in the rGO/NiO_x/Ag photocatalysis with the presence of MB molecules are given as follows:

$$e(CB) + O_2 \rightarrow O_2^{\cdot}$$

$$O_2^{\cdot} + H^+ \rightarrow {}^{\cdot}OOH$$

$$^{\cdot}OOH + {}^{\cdot}OOH \rightarrow H_2O_2 + O_2$$

$$H_2O_2 + O_2^{\cdot} \rightarrow {}^{\cdot}OH + OH^- + O_2$$

$$h^+ (VB) + H_2O \rightarrow {}^{\cdot}OH + H^+$$

$$h^+ (VB) + OH \rightarrow {}^{\cdot}OH$$

$$^{\cdot}OH + RH \rightarrow R^{\cdot} + H_2O$$

The PL (photoluminescence) spectra were used to determine the speed of photo-generated charge recombination in rGO, rGO/NiO_x, rGO/NiO_x/Ag, and nanocomposite (Fig. 8a). In PL profile of samples there are two main peaks at around 420 and

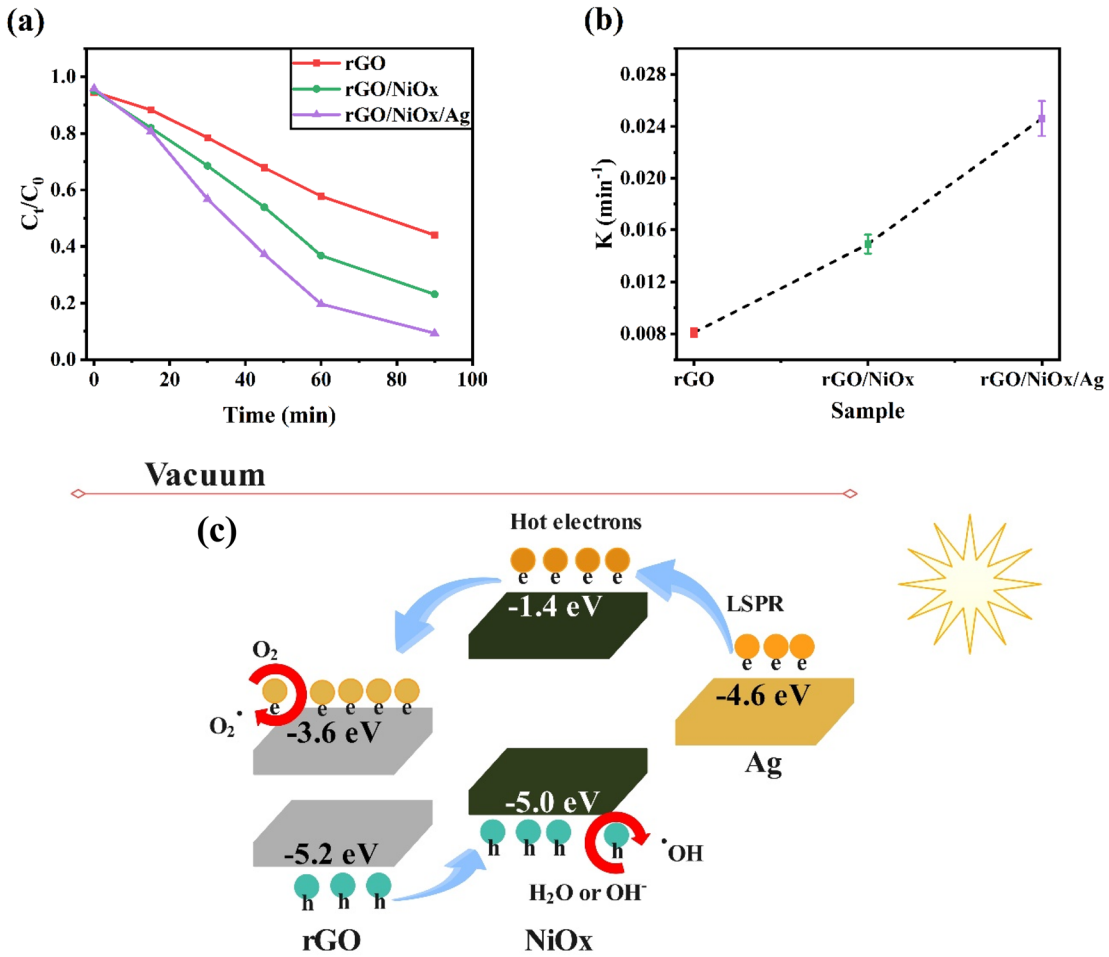

Fig. 7 (a) MB solutions photodegradation efficiency in the presence of different photocatalyst materials. (b) Corresponding photodegradation kinetic rate values of different samples. (c) Possible charge transfer mechanism in rGO/NiO_x/Ag photocatalyst during sunlight irradiance and degradation of methylene blue dye.

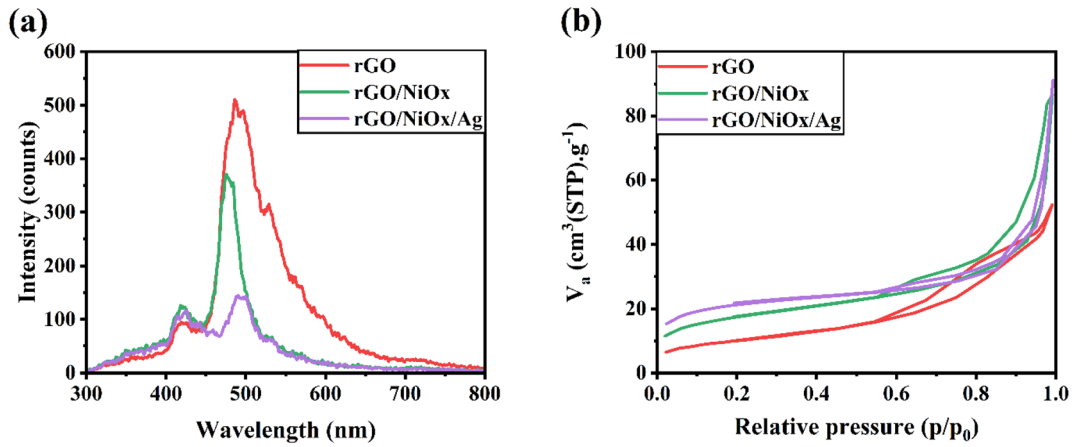

Fig. 8 (a) PL and (b) BET curves of different samples. Excitation wavelength to measure PL spectra was 240 nm.

485 nm, akin to the observed PL peaks material formed during reduction process[52] and the PL peak of 420 nm is due to the smaller sp^2 fragments.[53] The PL intensity of the rGO/NiO_x/Ag nanocomposite had been less than the rGO/NiO_x nanocomposite and rGO, indicating a lower rate of recombination and more carrier separation. This is due to both Ag-NPs and NiO_x-NPs exhibiting excellent electrical properties for the transport of electrons that are photoexcited and may function as

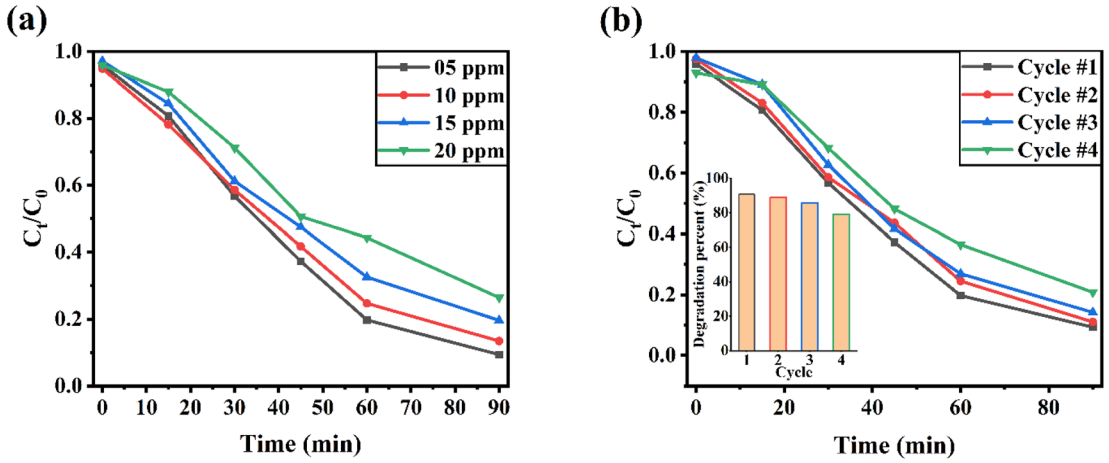

Fig. 9 (a) MB dye photodegradation efficiency with various concentrations in the presence of 50 mg L^{-1} of rGO/NiO_x/Ag ternary composites. (b) The reusability MB degradation performance of rGO/NiO_x/Ag system.

acceptors of electrons alongside rGO sheets. The addition of NiO_x and Ag to an rGO catalyst has a significant impact on electron–hole pair recombination and favors charge transfer at the interface, boosting the catalyst's stability. Furthermore, the mean pore diameter and specific area of the surface of the rGO, rGO/NiO_x, and rGO/NiO_x/Ag photocatalysts had been assessed using nitrogen adsorption–desorption curves generated from the BET test (Fig. 8b). The rGO, rGO/NiO_x, and rGO/NiO_x/Ag nanocomposite showed mean pore diameters of 8.99, 8.55, and 7.03 nm, respectively. In addition, their BET-specific surface area was 35.56, 60.83, and 76.05 m^2 g^{-1}, respectively. The obtained findings suggest that a higher specific area of the surface with a narrower pore width in the rGO/NiO_x/Ag nanocomposite may produce bigger active sites and mesopores, enabling photon and dye injection. These situations improve the materials' photocatalytic activity.[54,55]

Fig. 9a depicts the methylene blue dye removal effectiveness of rGO/NiO_x/Ag ternary composites *versus* time as the starting methylene blue dye concentration rose from 5 to 20 ppm. With increasing methylene blue dye concentration, the removal effectiveness of the rGO/NiO_x/Ag nanocomposite is lowered. In fact, at high methylene blue dye concentrations, the leftover methylene blue dye molecules rise when the absorbent capacity of the catalyst achieves equilibrium. As a result, a smaller number of photons contact the surface of the photocatalyst, leading to poor methylene blue dye photodegradation. The reusability of the ternary rGO/NiO_x/Ag material is examined by examining its photocatalytic performance for the MB degradation on four occasions under identical test circumstances (Fig. 9b). After four cycles, the degrading performance of the methylene blue dye dropped from 91% to 79%. The reusability test reveals that the developed ternary nanocomposite can be employed in the industry for long-term photodegradation.

Conclusion

In conclusion, the addition of NiO_x and Ag nanoparticles to rGO improved the photocatalytic degradation of methylene blue dye under simulated sunshine irradiation. The rGO/NiO_x/Ag nanocomposite had the greatest photoactivity (95%), which can be attributed to its excellent electron–hole pair separation rate. Furthermore, the k value of the rGO/NiO_x/Ag nanocomposite was discovered to be 0.024 min^{-1}, allowing for a threefold increase in photoactivity over rGO. Furthermore, after 4 cycles of repeating, the rGO/NiO_x/Ag nanocomposite retained a degradation efficiency greater than 79%, demonstrating its strong stability. This research introduced a novel approach to the design of composite photocatalysts with good charge separation and expanded their applications in environmental remediation.

Data availability

The data that support the findings of this study are available from the corresponding author upon reasonable request.

Conflicts of interest

The authors declare that they have no conflict of interest.

Acknowledgements

The author K. M Batoo would like to thank Researchers Supporting Project No. (RSP2024R148), King Saud University, Riyadh, Saudi Arabia for the financial support.

References

1 I. K. Konstantinou and T. A. Albanis, TiO_2-assisted photocatalytic degradation of azo dyes in aqueous solution: kinetic and mechanistic investigations: a review, *Appl. Catal., B*, 2004, **49**, 1–14.
2 F. Deng, L. Min, X. Luo, S. Wu and S. Luo, Visible-light photocatalytic degradation performances and thermal stability due to the synergetic effect of TiO_2 with

conductive copolymers of polyaniline and polypyrrole, *Nanoscale*, 2013, **5**, 8703–8710.

3 S. Xu, Y. Zhu, L. Jiang and Y. Dan, Visible light induced photocatalytic degradation of methyl orange by polythiophene/TiO_2 composite particles, *Water, Air, Soil Pollut.*, 2010, **213**, 151–159.

4 D. Wang, Y. Wang, X. Li, Q. Luo, J. An and J. Yue, Sunlight photocatalytic activity of polypyrrole–TiO_2 nanocomposites prepared by 'in situ'method, *Catal. Commun.*, 2008, **9**, 1162–1166.

5 M. Khanzadeh, M. Dehghanipour, A. Darehkordi and F. Rahmani, Wavelength-dependent nonlinear optical properties of 8-(4-methoxyphenyl)-6-oxo-3-p-tolyl-6H-pyrido [1, 2-b][1, 2, 4] triazine-7, 9-dicarbonitrile, *Can. J. Phys.*, 2018, **96**, 1288–1294.

6 A. Kumar and G. Pandey, A review on the factors affecting the photocatalytic degradation of hazardous materials, *Mater. Sci. Eng. C*, 2017, **1**, 1–10.

7 M. A. Brown and S. C. De Vito, Predicting azo dye toxicity, *Crit. Rev. Environ. Sci. Technol.*, 1993, **23**, 249–324.

8 S. Chen, J. Zhang, C. Zhang, Q. Yue, Y. Li and C. Li, Equilibrium and kinetic studies of methyl orange and methyl violet adsorption on activated carbon derived from Phragmites australis, *Desalination*, 2010, **252**, 149–156.

9 M. M. Khin, A. S. Nair, V. J. Babu, R. Murugan and S. Ramakrishna, A review on nanomaterials for environmental remediation, *Energy Environ. Sci.*, 2012, **5**, 8075–8109.

10 S. Parsons, *Advanced Oxidation Processes for Water and Wastewater Treatment*, IWA publishing, 2004.

11 J. C. Colmenares and R. Luque, Heterogeneous photocatalytic nanomaterials: prospects and challenges in selective transformations of biomass-derived compounds, *Chem. Soc. Rev.*, 2014, **43**, 765–778.

12 R. Rameshbabu, N. Kumar, A. Karthigeyan and B. Neppolian, Visible light photocatalytic activities of $ZnFe_2O_4$/ZnO nanoparticles for the degradation of organic pollutants, *Mater. Chem. Phys.*, 2016, **181**, 106–115.

13 N. Kumar, A. Sen, K. Rajendran, R. Rameshbabu, J. Ragupathi, H. A. Therese and T. Maiyalagan, Morphology and phase tuning of α-and β-MnO_2 nanocacti evolved at varying modes of acid count for their well-coordinated energy storage and visible-light-driven photocatalytic behaviour, *RSC Adv.*, 2017, **7**, 25041–25053.

14 M. Saleem, J. Iqbal, A. Nawaz, B. Islam and I. Hussain, Synthesis, characterization, and performance evaluation of pristine and cerium-doped WO_3 nanoparticles for photodegradation of methylene blue via solar irradiation, *Int. J. Appl. Ceram. Technol.*, 2020, **17**, 1918–1929.

15 C. Díaz, M. Segovia and M. L. Valenzuela, Solid state nanostructured metal oxides as photocatalysts and their application in pollutant degradation: a review, *Photochem*, 2022, **2**, 609–627.

16 G. Gnanamoorthy, V. K. Yadav, K. K. Yadav, K. Ramar, J. Alam, A. K. Shukla, F. A. A. Ali and M. Alhoshan, Fabrication of different SnO_2 nanorods for enhanced photocatalytic degradation and antibacterial activity, *Environ. Sci. Pollut. Res.*, 2021, 1–11.

17 A. A. Ezhilarasi, J. J. Vijaya, K. Kaviyarasu, L. J. Kennedy, R. J. Ramalingam and H. A. Al-Lohedan, Green synthesis of NiO nanoparticles using Aegle marmelos leaf extract for the evaluation of in-vitro cytotoxicity, antibacterial and photocatalytic properties, *J. Photochem. Photobiol., B*, 2018, **180**, 39–50.

18 M. A. Rahman, R. Radhakrishnan and R. Gopalakrishnan, Structural, optical, magnetic and antibacterial properties of Nd doped NiO nanoparticles prepared by co-precipitation method, *J. Alloys Compd.*, 2018, **742**, 421–429.

19 M. Ramesh, H. Nagaraja, M. P. Rao, S. Anandan and N. Huang, Fabrication, characterization and catalytic activity of α-MnO_2 nanowires for dye degradation of reactive black 5, *Mater. Lett.*, 2016, **172**, 85–89.

20 G. Gnanamoorthy, V. K. Yadav, D. Latha, V. Karthikeyan and V. Narayanan, Enhanced photocatalytic performance of $ZnSnO_3$/rGO nanocomposite, *Chem. Phys. Lett.*, 2020, **739**, 137050.

21 S. Dong, X. Ding, T. Guo, X. Yue, X. Han and J. Sun, Self-assembled hollow sphere shaped Bi_2WO_6/RGO composites for efficient sunlight-driven photocatalytic degradation of organic pollutants, *Chem. Eng. J.*, 2017, **316**, 778–789.

22 M. Khanzadeh, M. Dehghanipour, M. Karimipour and M. Molaei, Improvement of nonlinear optical properties of graphene oxide in mixed with Ag_2S@ZnS core-shells, *Opt. Mater.*, 2017, **66**, 664–670.

23 Q. A. Alsulami, A. Rajeh, M. A. Mannaa, S. M. Albukhari and D. F. Baamer, Preparation of highly efficient sunlight driven photodegradation of some organic pollutants and H_2 evolution over rGO/$FeVO_4$ nanocomposites, *Int. J. Hydrogen Energy*, 2021, **46**, 27349–27363.

24 H. Safajou, M. Ghanbari, O. Amiri, H. Khojasteh, F. Namvar, S. Zinatloo-Ajabshir and M. Salavati-Niasari, Green synthesis and characterization of RGO/Cu nanocomposites as photocatalytic degradation of organic pollutants in waste-water, *Int. J. Hydrogen Energy*, 2021, **46**, 20534–20546.

25 D. Deng, K. Novoselov, Q. Fu, N. Zheng, Z. Tian and X. Bao, Catalysis with two-dimensional materials and their heterostructures, *Nat. Nanotechnol.*, 2016, **11**, 218–230.

26 M. Faraji, M. Yousefi, S. Yousefzadeh, M. Zirak, N. Naseri, T. H. Jeon, W. Choi and A. Z. Moshfegh, Two-dimensional materials in semiconductor photoelectrocatalytic systems for water splitting, *Energy Environ. Sci.*, 2019, **12**, 59–95.

27 G. Gnanamoorthy, V. Karthikeyan, Z. Lu and V. Narayanan, Construction of $ZnNiO_2$/rGO nanocomposites with enhanced photocatalytic performance, *Inorg. Chem. Commun.*, 2023, **156**, 111203.

28 V. Etacheri, C. Di Valentin, J. Schneider, D. Bahnemann and S. C. Pillai, Visible-light activation of TiO_2 photocatalysts: Advances in theory and experiments, *J. Photochem. Photobiol. C: Photochem.*, 2015, **25**, 1–29.

29 M. Dehghanipour, M. Khanzadeh, M. Karimipour and M. Molaei, Dependence of nonlinear optical properties of Ag_2S@ZnS core-shells on Zinc precursor and capping agent, *Opt Laser. Technol.*, 2018, **100**, 286–293.

30 V. Thinh, V. Lam, T. Bach, N. Van, D. Manh, D. Tung, N. Lien, U. Thuy, T. Anh and N. Tung, Enhanced optical and photocatalytic properties of Au/Ag nanoparticle-decorated ZnO films, *J. Electron. Mater.*, 2020, **49**, 2625–2632.
31 S. Chidambaram, B. Pari, N. Kasi and S. Muthusamy, ZnO/Ag heterostructures embedded in Fe_3O_4 nanoparticles for magnetically recoverable photocatalysis, *J. Alloys Compd.*, 2016, **665**, 404–410.
32 M. Ahmad, E. Ahmed, Z. Hong, N. Khalid, W. Ahmed and A. Elhissi, Graphene–Ag/ZnO nanocomposites as high performance photocatalysts under visible light irradiation, *J. Alloys Compd.*, 2013, **577**, 717–727.
33 S. Koppala, Y. Xia, L. Zhang, J. Peng, Z. Chen and L. Xu, Hierarchical ZnO/Ag nanocomposites for plasmon-enhanced visible-light photocatalytic performance, *Ceram. Int.*, 2019, **45**, 15116–15121.
34 M. Kheirabadi, M. Samadi, E. Asadian, Y. Zhou, C. Dong, J. Zhang and A. Z. Moshfegh, Well-designed Ag/ZnO/3D graphene structure for dye removal: Adsorption, photocatalysis and physical separation capabilities, *J. Colloid Interface Sci.*, 2019, **537**, 66–78.
35 H. Mu, Y. Gu and H. Xie, Photocatalysis of Nickel-Based Graphene/Au/ZnO Nanocomposites, *IEEE Sens. J.*, 2019, **19**, 5376–5388.
36 P. Vivek, R. Sivakumar, E. S. Esakki and S. Deivanayaki, Fabrication of NiO/RGO nanocomposite for enhancing photocatalytic performance through degradation of RhB, *J. Phys. Chem. Solids*, 2023, **176**, 111255.
37 S. Lv, Y. Du, F. Wu, Y. Cai and T. Zhou, Review on LSPR assisted photocatalysis: effects of physical fields and opportunities in multifield decoupling, *Nanoscale Adv.*, 2022, **4**, 2608–2631.
38 A. M. Golsheikh, N. Huang, H. Lim and R. Zakaria, One-pot sonochemical synthesis of reduced graphene oxide uniformly decorated with ultrafine silver nanoparticles for non-enzymatic detection of H_2O_2 and optical detection of mercury ions, *RSC Adv.*, 2014, **4**, 36401–36411.
39 F. Arjmand, S. J. Fatemi, S. Maghsoudi and A. Naeimi, The first and cost effective nano-biocomposite, zinc porphyrin/CuO/reduced graphene oxide, based on Calotropis procera plant for perovskite solar cell as hole-transport layer under ambient conditions, *J. Mater. Res. Technol.*, 2022, **16**, 1008–1020.
40 A. C. Jeoffrey, S. J. Ramalingam, K. Murugaiah and A. Balu, One-pot green synthesis of rGO-NiO/CdO nanocomposite materials for the photocatalytic degradation of phenol from waste waters and the study of resistance against Staphylococcus aureus, *Hybrid Adv.*, 2023, 100064.
41 R. Vinoth, P. Karthik, K. Devan, B. Neppolian and M. Ashokkumar, TiO_2–NiO p–n nanocomposite with enhanced sonophotocatalytic activity under diffused sunlight, *Ultrason. Sonochem.*, 2017, **35**, 655–663.
42 F. Kayaci, S. Vempati, C. Ozgit-Akgun, I. Donmez, N. Biyikli and T. Uyar, Selective isolation of the electron or hole in photocatalysis: ZnO–TiO_2 and TiO_2–ZnO core–shell structured heterojunction nanofibers via electrospinning and atomic layer deposition, *Nanoscale*, 2014, **6**, 5735–5745.
43 S. Ma, J. Xue, Y. Zhou and Z. Zhang, Photochemical synthesis of ZnO/Ag_2O heterostructures with enhanced ultraviolet and visible photocatalytic activity, *J. Mater. Chem. A*, 2014, **2**, 7272–7280.
44 M. Deo, D. Shinde, A. Yengantiwar, J. Jog, B. Hannoyer, X. Sauvage, M. More and S. Ogale, Cu_2O/ZnO hetero-nanobrush: hierarchical assembly, field emission and photocatalytic properties, *J. Mater. Chem.*, 2012, **22**, 17055–17062.
45 T. K. Das, S. K. Ghosh and N. C. Das, Green synthesis of a reduced graphene oxide/silver nanoparticles-based catalyst for degradation of a wide range of organic pollutants, *Nano-Struct. Nano-Objects*, 2023, **34**, 100960.
46 H. S. Ahn, J.-W. Jang, M. Seol, J. M. Kim, D.-J. Yun, C. Park, H. Kim, D. H. Youn, J. Y. Kim and G. Park, Self-assembled foam-like graphene networks formed through nucleate boiling, *Sci. Rep.*, 2013, **3**, 1396.
47 N. Kumar, J. R. Rodriguez, V. G. Pol and A. Sen, Synergistically advancing Li storage property of hydrothermally grown 1D pristine MnO_2 over a mesh-like interconnected framework of 2D graphene oxide, *J. Solid State Electrochem.*, 2019, **23**, 1443–1454.
48 P. Ravikumar, B. Kisan and A. Perumal, Enhanced room temperature ferromagnetism in antiferromagnetic NiO nanoparticles, *AIP Adv.*, 2015, **5**, 087116.
49 M. Ikram, A. Raza, M. Imran, A. Ul-Hamid, A. Shahbaz and S. Ali, Hydrothermal synthesis of silver decorated reduced graphene oxide (rGO) nanoflakes with effective photocatalytic activity for wastewater treatment, *Nanoscale Res. Lett.*, 2020, **15**, 1–11.
50 M. Kocijan, L. Ćurković, G. Gonçalves and M. Podlogar, The potential of rGO@TiO_2 photocatalyst for the degradation of organic pollutants in water, *Sustainability*, 2022, **14**, 12703.
51 J. Tian, X. Cao, T. Sun, J. Fan, H. Miao, Z. Chen, D. Li, E. Liu and Y. Zhu, S-scheme $Co_3(PO_4)_2$/Twinned-$Cd_{0.5}Zn_{0.5}S$ homo-heterojunction for enhanced photocatalytic H_2 evolution, *Chem. Eng. J.*, 2023, **471**, 144587.
52 C. T. Chien, S. S. Li, W. J. Lai, Y. C. Yeh, H. A. Chen, I. S. Chen, L. C. Chen, K. H. Chen, T. Nemoto and S. Isoda, Tunable photoluminescence from graphene oxide, *Angew. Chem., Int. Ed.*, 2012, **51**, 6662–6666.
53 G. Eda, Y. Y. Lin, C. Mattevi, H. Yamaguchi, H. A. Chen, I. S. Chen, C. W. Chen and M. Chhowalla, Blue photoluminescence from chemically derived graphene oxide, *Adv. Mater.*, 2010, **22**, 505–509.
54 L. Zhang, H. Qi, Y. Zhao, L. Zhong, Y. Zhang, Y. Wang, J. Xue and Y. Li, Au nanoparticle modified three-dimensional network PVA/RGO/TiO_2 composite for enhancing visible light photocatalytic performance, *Appl. Surf. Sci.*, 2019, **498**, 143855.
55 W. Zhang, X. Xiao, L. Zheng and C. Wan, Fabrication of TiO_2/MoS_2@zeolite photocatalyst and its photocatalytic activity for degradation of methyl orange under visible light, *Appl. Surf. Sci.*, 2015, **358**, 468–478.